

Adsorption of gold atoms on the *h*-BN/Rh(111) nanomesh

Hans Peter Koch, Robert Laskowski, Peter Blaha, and Karlheinz Schwarz

Institute of Materials Chemistry, Vienna University of Technology, Getreidemarkt 9/165-TC, A-1060 Vienna, Austria

(Received 19 September 2011; revised manuscript received 24 November 2011; published 9 December 2011)

We present density functional calculations of the adsorption of a single Au atom on the *h*-BN/Rh(111) nanomesh and compare it to Au adsorption on a pure *h*-BN surface. While Au binds only weakly to pure *h*-BN (similar to graphene) or to BN at the “wires” of the nanomesh, the subsurface Rh atoms in the “pores” of the nanomesh modify the electronic structure of *h*-BN considerably and Au adsorbs strongly on top of the B atoms. A large outward relaxation of the B atom accompanies the strong covalent interaction and, in addition, the Au atoms are significantly charged. The results provide a first explanation of the ability of the *h*-BN nanomesh to trap small metal clusters in its pores.

DOI: [10.1103/PhysRevB.84.245410](https://doi.org/10.1103/PhysRevB.84.245410)

PACS number(s): 73.20.At, 68.37.Ef, 73.22.-f

I. INTRODUCTION

The adsorption of hexagonal boron nitride (*h*-BN) on metal surfaces has been studied for many years both theoretically and experimentally.^{1–5} This interest was driven mainly by the ability of boron nitride to form ultrathin well-ordered monolayers, protecting the underlying substrate against oxidation. Moreover, *h*-BN was found to bind to a quite large number of substrates, even when the lattice constants of *h*-BN and the substrate do not match. The prototypical example is the *h*-BN/Ni(111) interface, which has nice lattice matching and forms a simple epitaxial 1×1 structure. It is prepared by thermal decomposition of borazine $B_3H_6N_3$ on a hot Ni(111) surface. Aside from Ni(111),^{2,3,6–8} a simple epitaxial 1×1 *h*-BN monolayer was also successfully deposited on Cu(111).⁹ It has been confirmed by density functional theory (DFT) calculations that for the commensurate interfaces, the energetically most stable structure have N atoms on top of the metal atoms, while the B atoms can occupy the fcc or hcp positions,⁶ leading to two domains those have also been observed experimentally. These *h*-BN monolayers are not completely flat, but undergo a small buckling of about 0.1 Å where the N atoms are pushed away from the surface, whereas the B atoms are attracted by the underlying metal atoms.⁶ It is believed that the rigid *sp*² bonds between N and B in the hexagonal plane are not considerably weakened,³ although the interaction between *h*-BN and the substrate is relatively strong.⁸

In the case of incommensurate interfaces (where the lattice constants of *h*-BN and the metal substrate do not match), the mismatch can lead to some extraordinary structures. Corso *et al.*¹⁰ have reported the formation of a self-assembled nanostructure, the so-called nanomesh, on the lattice-mismatched Rh(111) surface with a periodicity of about 3.2 nm. This corresponds to a situation where the lattice of 12×12 Rh(111) matches 13×13 *h*-BN cells forming the periodic nanomesh structure, which is caused by the lattice-mismatch between Rh(111) and *h*-BN as mentioned above. In addition, the nanomesh possesses two distinct *h*-BN regions: hexagonally arranged pores surrounded by so-called wires with a large corrugation of 1 to 2 Å. These pores have a diameter of about 2 nm.^{11,12} Initially, the STM images and the observed σ -band splitting of about 1 eV was explained by a double-layer model, which consists of two, partially incomplete *h*-BN layers.

Later on, DFT calculations showed that the STM images as well as the splitting of the σ bands can be explained by a highly corrugated *h*-BN monolayer.^{13,14} In this context, it would be more appropriate to call the nanomesh a strong Moire pattern. In this “single-layer” model, the two regions observed experimentally can be explained by different *h*-BN adsorption configurations, i.e., the positions of the B or N atoms relative to the underlying metal surface. The “pores” are formed when *h*-BN stays close to the substrate and N atoms are located close to the top position, whereas the “wires” are regions where *h*-BN is repelled because N atoms are close to the hcp or fcc position.^{13,15} Since the first discovery of the nanomesh¹⁰ on the Rh(111) surface, similar structures have also been found on Ru(0001),¹⁶ Pd(111),¹⁷ Pd(110),¹⁸ and Pt(111). Aside from *h*-BN, similar nanostructured patterns have also been found after deposition of graphene on transition-metal surfaces.^{19–22} Both graphene and boron nitride are possible components for engineering future nanoelectronic devices.²³

The local electronic structures of the pores and wires are quite different, which, for example, becomes apparent in the splitting of the σ band by about 1 eV. Therefore, one expects that these regions will also show a different adsorption behavior. In fact, Dil *et al.*¹² have found that Xe atoms prefer to adsorb at the rim of pores. According to DFT calculations, this area at the borderline between the differently charged pores and wires has a large electric field gradient, resulting in a stronger attraction of the Xe atoms. Recently, this preference was confirmed by Widmer *et al.*²⁴ Similarly, molecules such as naphthalocyanine have been successfully deposited on the *h*-BN/Rh(111) nanomesh¹¹ and are immobilized within the pores. Moreover, it has been shown that the pores of the *h*-BN nanomesh on Ru(0001) (Ref. 16) or Rh(111) (Ref. 25) can accommodate Au or Co clusters.²⁶ The ability to form ordered arrays of small metal clusters, which are prevented to segregate into larger ones because they are trapped within the pores, makes the nanomesh a possible candidate as a nanostructured template for catalysis.

In order to gain some theoretical insight into the adsorption of metal atoms, and as a first step, we investigate in this paper the adsorption of a single Au atom on a surface of bulk *h*-BN and compare it to the adsorption of Au on the *h*-BN/Rh(111) nanomesh.

II. STRUCTURE MODELS

The h -BN/Rh(111) nanomesh consists of a 13×13 supercell of h -BN on top of a 12×12 supercell of Rh(111),¹⁴ and even when the metal is simulated with just three layers, such a structure contains more than 1000 atoms per cell. Such sizes require very large computational resources and thus we approximate in most calculations the large nanomesh unit cell by smaller models in order to save computer time. As already mentioned in the Introduction, h -BN in the pores of the nanomesh is attracted to the metal substrate and stays relatively close to it. In this region, the N atoms are nearly on top of the metal atoms and the B atoms are in fcc positions [black frame in Fig. 1(a)]. Thus, we will call this configuration as BN(fcc,top) [see Fig. 1(c)]. In the wire region of the nanomesh, h -BN is repelled from the underlying surface and the h -BN

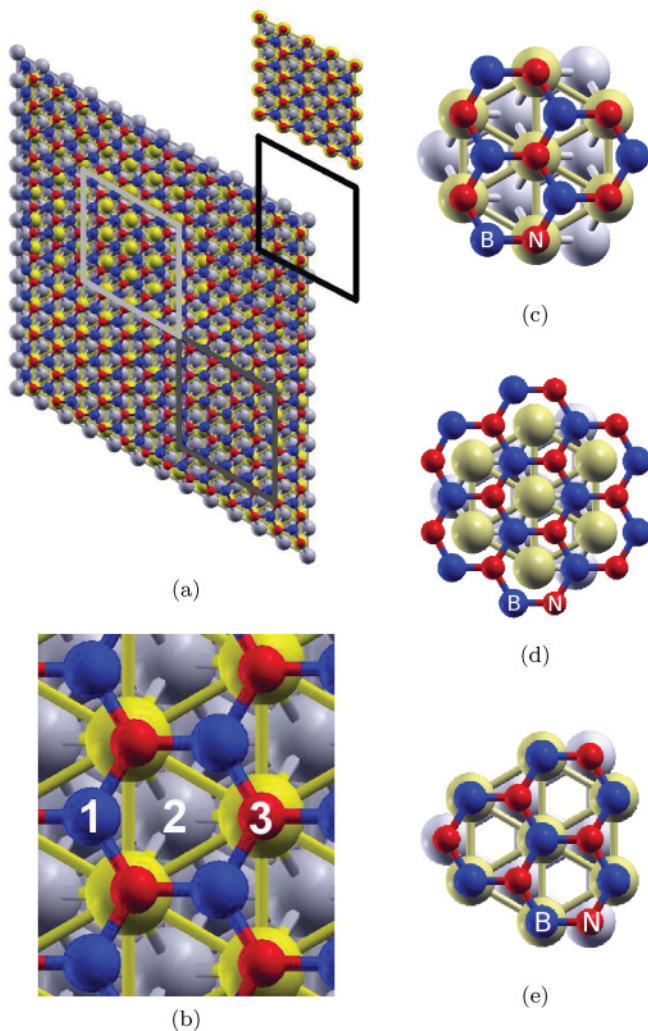


FIG. 1. (Color online) Geometric details of the studied structures (N: red; B: blue; Rh first and second layers: yellow and gray spheres): (a) comparison between the unit cell of the full h -BN/Rh(111) nanomesh and the small 4×4 unit-cell models (the black, dark, and light gray frames indicate the areas that are approximated by the small cells); (b) the three investigated adsorption sites of gold, where Au is located at (1) B_{top} , (2) BN_{hollow} , and (3) N_{top} ; (c) BN(fcc,top) strongly bound to Rh; (d) BN(hcp,fcc) weakly bound to Rh; (e) BN(top,hcp) weakly bound to Rh.

TABLE I. Distances (in Å) between the Rh surface and B (z_B) and N (z_N) and between B and N (d_{B-N}) of h -BN(fcc, top)/Rh(111) when using the h -BN or the Rh lattice parameters with the corresponding average distances in the center of the pores of the 13×12 h -BN/Rh(111) nanomesh. In all calculations, the WC functional was used.

System	z_B	z_N	d_{B-N}
h -BN/Rh(111) _{h-BN}	2.27	2.37	1.44
h -BN/Rh(111) _{Rh}	2.07	2.21	1.55
13×12 h -BN/Rh(111)	2.10	2.23	1.47

layer is buckled away from the metal. In this case, the B and N atoms are close to the hcp and fcc [light gray frame in Fig. 1(a)] or top and fcc positions [dark gray frame in Fig. 1(a)], respectively, or in short notation BN(hcp, fcc) or BN(top, fcc) [see Figs. 1(d) and 1(e)]. The transition between wires and pores is rather sharp and occurs nearly within one or two BN bond lengths. Therefore, we can model these regions by smaller 4×4 h -BN/metal supercells [as indicated above the black frame of Fig. 1(a)], which we denote below by BN(fcc, top), BN(hcp, fcc), or BN(top, fcc), respectively [see Figs. 1(c)–1(e)]. Since there is an 8% lattice mismatch between h -BN and Rh(111), we have either to stretch h -BN or compress Rh(111) to make them commensurate. Both approximations have been investigated and will be discussed later on. Some quantitative differences are present, but the main conclusions do not depend on this choice.

The 4×4 cell has been chosen in order to ensure that the adsorbed Au atoms are well separated. The metal substrate consists of three layers covered on both sides with a h -BN layer (for inversion symmetry and real matrix elements). A vacuum region of about 15 Å separates the h -BN layers.

Table I lists in the first two lines the distances of the N and B atoms from the metal surface for the commensurate 4×4 unit cells when using the h -BN (this corresponds to compressed Rh) or Rh lattice parameters (stretched h -BN). In the third line, we give the results for the pores of the full 13×12 nanomesh. We observe that both N and B atoms are further away from the surface when the h -BN lattice parameter is used, whereas in the other case, the B-N distance is much too large. The latter influences the BN properties (and thus the Au-adsorption on h -BN) much more than when using the original h -BN lattice parameter. Therefore, we use the h -BN lattice parameter for most of our 4×4 supercell calculations.

III. COMPUTATIONAL METHOD

All *ab initio* calculations have been carried out within DFT using the augmented plane waves plus local orbitals method (APW + lo),²⁷ as implemented in the WIEN2K package.²⁸ For some of the investigated structures, van der Waals interactions could be of some importance. In order to check how much the results depend on the exchange-correlation potential, we use the local density approximation (LDA) and the more recent Wu-Cohen (WC) generalized gradient approximation (GGA).^{29–31} Since LDA usually leads to overbinding, but GGAs tend to underbinding, these functionals may set the

boundaries for results using a properly van der Waals corrected DFT.

The Brillouin zone was sampled with a $2 \times 2 \times 1$ mesh of k points. In the case of density of states (DOS) calculations, the k -grid was increased to a $4 \times 4 \times 1$ mesh. The APW + l basis set quality was determined by RKmax 5.0 with muffin-tin radii of 1.17, 0.61, 0.81, and 1.22 Å for Rh, B, N, and Au, respectively.

Figure 1(b) shows the three investigated adsorption sites of gold in the three 4×4 unit cells: (1) Au on top of a B atom (B_{top}), (2) Au in the center of a surrounding h -BN ring (BN_{hollow}), and (3) Au on top of an N atom (N_{top}). During geometry optimization, the Au atom was allowed to move only vertically, while its planar coordinates were constrained. In case of Au on B_{top} and N_{top} , the N or B atoms directly below Au were also allowed to move only vertically.

The results for the constraint 4×4 supercell were verified by a few calculations using the full nanomesh unit cell 13×13 h -BN on 12×12 Rh(111) [see Fig. 1(b)]. The model of the nanomesh was taken from the DFT calculations of Laskowski and Blaha.^{14,32} Only the 10 closest atoms around a single Au atom were allowed to change their positions to minimize the computational cost. In addition, we also tested a case in which the Au atom was moved to the rim of the pores in order to check whether or not the preferred adsorption site of Au is eventually at an edge of the pores (as for Xe). Such a configuration can not be approximated by the small unit cells.

The adsorption energy (E_{ads}) is calculated according to

$$E_{\text{ads}} = E_{\text{Au}} + E_{h\text{-BN/Rh}} - E_{\text{Au}/h\text{-BN/Rh}}, \quad (1)$$

where E_{Au} is the total energy of a single (spin-polarized) gold atom and $E_{\text{Au}/h\text{-BN/Rh}}$ and $E_{h\text{-BN/Rh}}$ are the total energies of

h -BN/Rh with and without the gold atom adsorbed, respectively. A positive value means a favorable adsorption.

IV. RESULTS AND DISCUSSION

A series of structure optimizations was carried out using the 4×4 supercells described above. Table II collects the adsorption energies of a Au atom on various surfaces and the distances between the Au and the nearest B and N atoms as well as their displacements due to the presence of the Au atom. The calculations have been done for a pure h -BN surface as well as for h -BN/Rh(111) in several configurations [nonbonding BN(hcp, fcc) and BN(top, hcp) and bonding BN(fcc, top)]. The h -BN/Rh(111) interface has been constructed using compressed metal layers such that it matches the h -BN lattice constant. Because the WC-GGA functional yields a much too small interaction between the hexagonal planes of bulk h -BN,³⁰ we show the results for the LDA exchange correlation functional. We have tested three adsorption sites shown in Fig. 1(b): B-top, N-top, and BN-hollow (in the center of the h -BN ring).

For a pure h -BN surface, the interaction with Au is quite weak and the Au adsorption energy is only 0.36 eV for both, Au on top of N or B, while for the hollow site, the adsorption energy is even a bit smaller. Since h -BN is insulating, the Au atom keeps a small spin polarization. Only for Au in the B-top position is the surface h -BN layer a bit disturbed and the B atom moves 0.1 Å toward the Au atom. These results are quite similar to the case of Au adsorbed on graphene.³³ The binding energy of Au on top of a carbon atom is even smaller than that of Au on h -BN, while the Au-C distance is about 2.5 Å, a value right in-between the distances of Au-B and Au-N (Table II).

TABLE II. Adsorption energies E_{ads} (in eV) and geometric properties (in Å) for various Au adsorption sites (B_{top} , N_{top} and BN_{hollow}) on various substrates [bulk h -BN, BN(hcp, fcc)/Rh(111) _{h -BN}, BN(top, hcp)/Rh(111) _{h -BN} and BN(fcc, top)/Rh(111) _{h -BN}]. $d_{\text{B-Au}}$ and $d_{\text{N-Au}}$ are averaged distances between Au and the nearest B and N atoms. Δz_{B} and Δz_{N} are averaged changes in height of the surface B and N atoms close to the adsorbed Au atom and z_{Au} is the height of Au with respect to the h -BN layer. All results are obtained using LDA and a compressed Rh surface.

Au site	$d_{\text{B-Au}}$	$d_{\text{N-Au}}$	Δz_{B}	Δz_{N}	z_{Au}	E_{ads}
Bulk h -BN						
B_{top}	2.31	2.82	+0.13	+0.02	2.42	0.36
N_{top}	2.76	2.36	+0.03	+0.01	2.36	0.36
BN_{hollow}	2.76	2.80	+0.02	-0.03	2.36	0.22
BN(hcp, fcc)/Rh(111) _{h-BN}						
B_{top}	2.25	2.78	+0.05	-0.08	2.30	0.72
N_{top}	2.68	2.27	+0.00	-0.03	2.24	0.74
BN_{hollow}	2.71	2.75	-0.04	-0.10	2.25	0.70
BN(top, hcp)/Rh(111) _{h-BN}						
B_{top}	2.25	2.79	+0.05	-0.10	2.29	0.75
N_{top}	2.69	2.28	-0.01	-0.04	2.24	0.73
BN_{hollow}	2.72	2.76	-0.03	-0.10	2.28	0.58
BN(fcc, top)/Rh(111) _{h-BN}						
B_{top}	2.09	2.90	+0.47	-0.06	2.51	2.40
N_{top}	2.56	2.51	+0.25	-0.23	2.29	1.69
BN_{hollow}	2.57	2.78	+0.21	-0.12	2.33	1.66

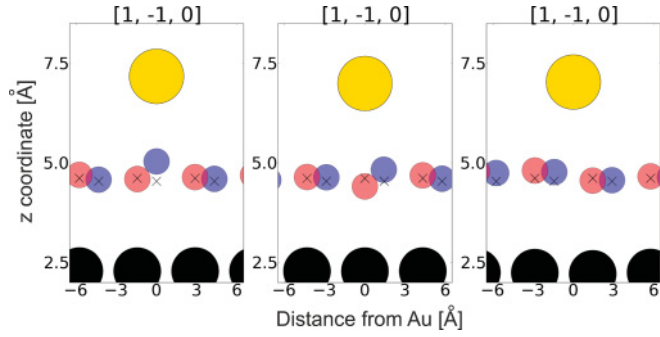


FIG. 2. (Color online) Height of Au and neighboring atoms (in Å) for Au on top of B (left), Au on top of N (middle), and Au in hollow position (right) for the 4×4 BN(fcc,top)/Rh(111)_{*h*-BN} system in planes as indicated in the figures. Au: yellow; B: blue; N: red; and Rh: black spheres. The crosses indicate the B and N positions without Au.

For the *h*-BN/Rh(111) nanomesh (in the 4×4 supercell models), the calculated adsorption energies increase and become very different for the bonding [BN(fcc,top)] and nonbonding *h*-BN/Rh(111) configurations. The values for both nonbonding *h*-BN/Rh(111) configurations [BN(hcp,fcc) and BN(top,hcp)] are about 0.7 eV and, similar to the pure *h*-BN surface, there is not much difference between the Au positions on B-top, N-top, and BN-hollow. The *h*-BN surface layer is not much affected and only a very small tendency for outward or inward buckling of B/N can be seen. On average, the distance of the Au atom from the surface is reduced by only 0.1 Å as compared to the bulk *h*-BN surface, but on that surface, the Au atom is no longer magnetic. Additionally, it should be noted that we have not taken into account possible van der Waals interactions. Their considerations could have some effect on the small adsorption energies of Au at the bulk *h*-BN and at the nonbonding *h*-BN/Rh(111) configurations, but this will not change any conclusions.

However, for the bonding BN(fcc,top) configuration, the adsorption energies increase considerably and there is a clear preference for the Au atom at the B-top position (2.4 eV) as compared to the N-top and hollow sites (1.7 eV), respectively. In all cases, the surface B atom(s) close to the Au atom move significantly outward (see Fig. 2). For the Au on B-top position (Fig. 2, left), the B atom moves 0.5 Å toward Au, while the neighboring N atom(s) move slightly in the opposite direction. On the other hand, when Au sits on top of N (Fig. 2, middle),

this N atom is pushed down (0.25 Å), while the neighboring three B atoms move 0.25 Å toward Au. A similar (but weaker) effect can be seen when Au sits in the hollow position (Fig. 2, right). Note that, without adsorbed Au atoms, the B and N atoms are slightly buckled in the opposite direction, i.e., the B atom is about 0.1 Å closer to Rh than N.

These results reveal a clear trend, namely, that Au atoms will preferentially adsorb on top of B atoms in the pores of the *h*-BN nanomesh (and not at the wires). Since the adsorption energy of a single Au atom is smaller than the cohesive energy of fcc-Au (3.81 eV), we can expect some aggregation of Au atoms. However, due to the small adsorption energy at the wires of the nanomesh of only 0.7 eV (see Table II), the diffusion barrier is rather high and may already explain the ability of the *h*-BN nanomesh to form well-ordered arrays of Au clusters in the pores, which are hindered to segregate at moderate temperatures.

As mentioned in Sec. III, the results might be affected by the choice of the exchange-correlation functional and the in-plane lattice parameter of the *h*-BN/Rh(111) interface (in the commensurate interface, we can select either the optimized Rh or *h*-BN lattice parameter). A comparison of the results using two functionals (LDA or WC) and two lattice parameters (Rh or *h*-BN) for the Au adsorption on the bonding BN(fcc,top)/Rh(111) nanomesh is given in Table III. We observe that LDA leads to a roughly 20% bigger adsorption energy compared to the WC-GGA. Also, the choice of the surface lattice parameter affects the energies by about 20%. The interface with the compressed metal surface (*h*-BN lattice parameter) leads to bigger adsorption energies. The trends are similar for other adsorption configurations and interfaces. As expected, LDA always leads to slightly smaller bond distances. On the other hand, the smaller *h*-BN lattice parameter causes larger Au-B(N) distances for the corresponding Au-top configurations. This effect is in particular large for the rather long N-Au distance in the N-top configuration. On average, the effects are not negligible on a quantitative level, but qualitatively there is no change and thus the specific choices do not affect the final conclusions. As will be seen at the end of this chapter, calculations using the *h*-BN lattice parameters agree better with the results obtained for the full nanomesh.

The electronic structure of bulk *h*-BN can be characterized by bonding (occupied) and antibonding (unoccupied) σ (p_x and p_y) and π (p_z) states. The σ states have obviously a much larger bonding-antibonding splitting and thus are much lower

TABLE III. Adsorption energies E_{ads} (in eV) and geometric properties (in Å) for various Au adsorption sites (B_{top}, N_{top}, and BN_{hollow}) on BN(fcc,top)/Rh(111) with either *h*-BN or Rh lattice parameters using LDA and WC-GGA. For further definitions, see Table II.

	Au site	BN(fcc, top)/Rh(111) _{<i>h</i>-BN}					BN(fcc, top)/Rh(111) _{Rh}						
		$d_{\text{B-Au}}$	$d_{\text{N-Au}}$	Δz_{B}	Δz_{N}	z_{Au}	E_{ads}	$d_{\text{B-Au}}$	$d_{\text{N-Au}}$	Δz_{B}	Δz_{N}	z_{Au}	E_{ads}
LDA	B _{top}	2.09	2.90	+0.47	-0.06	2.51	2.40	2.07	2.92	+0.51	-0.02	2.49	2.05
	N _{top}	2.56	2.51	+0.25	-0.23	2.29	1.69	2.91	2.36	+0.06	+0.03	2.44	1.06
	BN _{hollow}	2.57	2.78	+0.21	-0.12	2.33	1.66	2.67	2.78	+0.23	-0.02	2.31	1.14
WC	B _{top}	2.13	2.95	+0.49	-0.06	2.54	1.98	2.09	2.95	+0.52	-0.01	2.53	1.68
	N _{top}	2.57	2.58	+0.29	-0.24	2.31	1.37	2.97	2.47	+0.07	-0.02	2.52	0.71
	BN _{hollow}	2.70	2.90	+0.19	-0.11	2.38	1.30	2.88	2.94	+0.18	-0.01	2.53	0.78

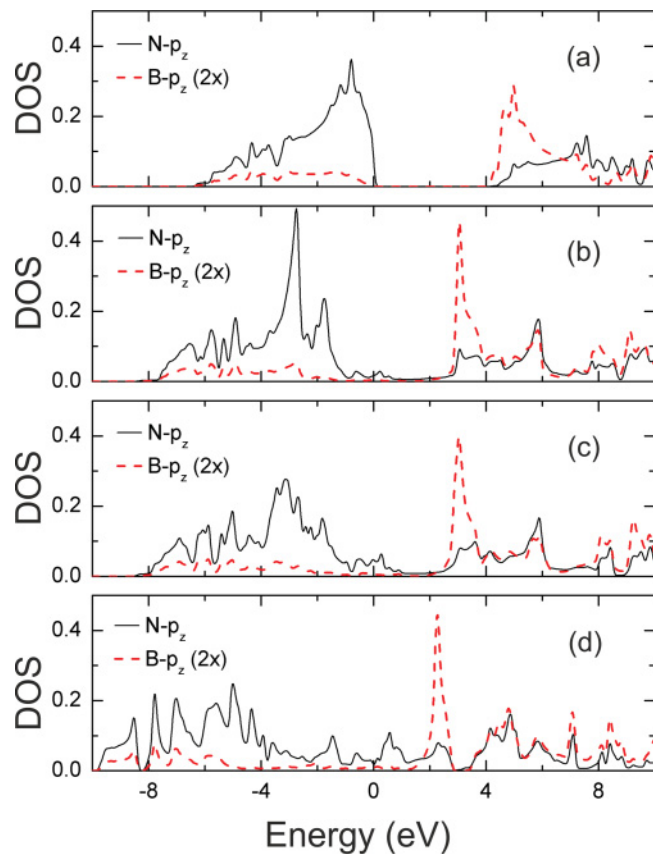


FIG. 3. (Color online) Partial DOS (using LDA) of the $N-p_z$ and $B-p_z$ (scaled by a factor of 2) states of (a) bulk BN, (b) nonbonding BN(hcp,fcc)/Rh(111)_h-BN, (c) BN(top,hcp)/Rh(111)_h-BN, and (d) bonding BN(fcc,top)/Rh(111)_h-BN nanomesh. The Fermi energy (E_F) is set to 0 eV.

(higher) in energy than the corresponding π states. Around the Fermi energy (E_F), the π states dominate. Due to the different electronegativity of B and N, the $N-p_z$ states dominate at the valence-band maximum (VBM), while the conduction-band minimum (CBM) has stronger $B-p_z$ character. In GGA calculations, the gap in bulk BN is about 4.2 eV [Fig. 3(a)]. The bonding of h -BN to the metal surface is driven by the hybridization of the $N-p_z$ and $B-p_z$ states with the metal d_{z^2} states.¹⁵ As a result, the p_z projected DOS in the various h -BN/Rh(111) interfaces are eventually modified compared to pure h -BN. Figure 3 visualizes the effects showing the N - and $B-p_z$ projected density of states. For nonbonding h -BN/Rh(111) configurations, the modification of the partial π DOS is relatively weak. The gap for the BN- π states basically is still present and E_F lies inside this gap [Figs. 3(b) and 3(c)]. On the other hand, the effect of the Rh(111) subsurface on the h -BN states is much stronger when BN is in the bonding configuration [BN(fcc,top)/Rh(111), Fig. 3(d)] and, in particular, the $N-p_z$ states are spread out over the whole energy range due to strong bonding-antibonding p_z - d_{z^2} interactions with the Rh states. Due to these interactions, the distance between the h -BN and the metal surface is quite small for the bonding configuration, resulting in a sizable charge transfer toward the h -BN.³² Of course, these modifications of the BN electronic structure affects the adsorption of a Au atom on

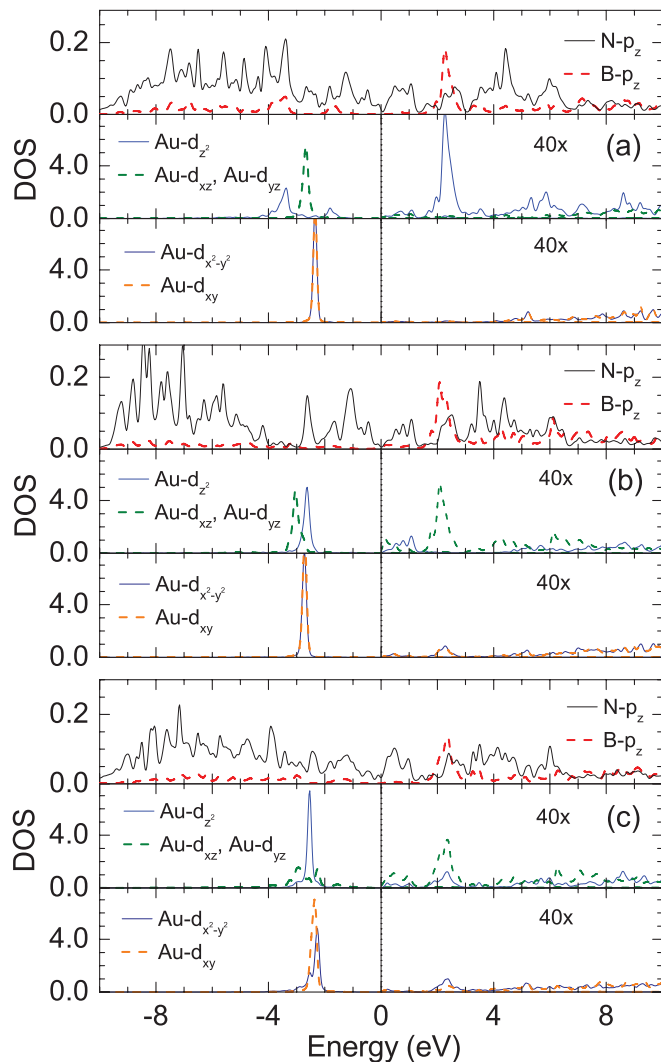


FIG. 4. (Color online) Calculated projected density of states (using WC-GGA) of $B-p_z + N-p_z$, $Au-d_{z^2}$, $Au-d_{xz} + Au-d_{yz}$, and $Au-d_{xy} + Au-d_{x^2-y^2}$ states for the three investigated Au adsorption sites on bonding BN(fcc,top)/Rh(111)_h-BN: (a) Au on B_{top} , (b) Au on N_{top} , and (c) Au on BN_{hollow} . The partial Au-DOS above E_F (0 eV) has been scaled for better visibility of the small antibonding contributions.

h -BN and explains the strong preference to adsorb only in the nanomesh “hole” areas.

In order to gain further insight into the bonding of a Au atom to the h -BN/Rh(111) nanomesh, we first look at the projected density of states corresponding to the $N-p_z$, $B-p_z$, and Au- d character (Fig. 4). Here, we focus only on the bonding BN(fcc,top) configuration. In all cases, the partial Au d_{xy} and $d_{x^2-y^2}$ DOS exhibits sharp peaks around -2.5 eV but hardly any signs of interactions with h -BN orbitals. More interesting is the Au- d_{xz} , $-d_{yz}$, and $-d_{z^2}$ DOS. When Au sits on top of B [B_{top} adsorption site, Fig. 4(a)], the Au- d_{z^2} DOS is fairly broad and seems to coincide with both B and $N-p_z$ states (peaks around -3.5 and $+2$ eV), indicating a covalent interaction between these orbitals with splittings into bonding and antibonding states. The latter are unoccupied, but notice the largely enhanced scale for this part of the DOS (Fig. 4).

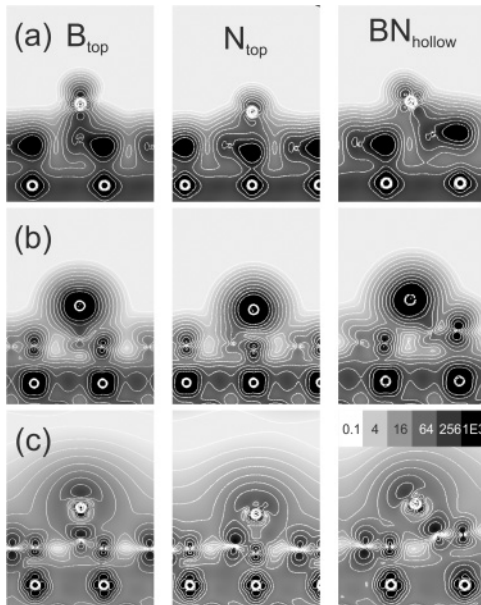


FIG. 5. Charge density distribution (in e/bohr^3) in a plane through Au and the nearest BN (and Rh) atoms (see also Fig. 2). The densities are shown for three Au adsorption sites (B_{top} , N_{top} , and BN_{hollow}) on $BN(\text{fcc,top})/\text{Rh}(111)_{h\text{-BN}}$ using the WC-GGA. (a) for states from -9 to -4 eV; (b) from -4 eV to E_F ; (c) from E_F to 4 eV.

Later on, we will use the charge density to get more insight into the bonding or antibonding character of this interaction. For the N-top site [Fig. 4(b)], the Au- d_{z^2} projected DOS is localized closer to E_F and has a smaller splitting (at -2.7 eV and just above E_F). Furthermore, it coincides only with N- p_z states, but not with B- p_z . For the hollow site [BN_{hollow} , Fig. 4(c)], there is hardly any coincidence with N or B states in the occupied part of the DOS, resulting in a very sharp peak at about -2.5 eV. On the other hand, the situation for the Au- d_{xz} , d_{yz} states is basically inverted. For Au on the B-top site, there is not much interaction between these states and B or N- p_z , and these states are fully occupied. However, for N-top and hollow sites, these states are broader in the occupied region and in addition there is substantial DOS in the unoccupied region (around 2 eV), coinciding mainly with B- p_z states.

While the DOS analysis can only provide hints about possible covalent interactions due to common peaks, it can not tell whether this interaction is bonding or antibonding. For this purpose, one needs to investigate either directly the (complex) wave function of selected states or one can check the electron density calculated from states in a certain energy window below and above E_F . Figures 5(a) and 5(b) show the densities originating from states in energy regions -9 to -4 eV, and -4 eV to E_F , respectively. In the lowest-energy region [Fig. 5(a)], the B-N σ bands dominate as indicated by the high density between these atoms. Nevertheless, both B and N atoms have a bonding interaction with the Au atom in all three geometric configurations. However, the Au character is rather weak (actually, it is so small that in this energy region, the Au partial DOS is hardly visible in Fig. 4), but still one can see that the charge density between B and Au is larger than between N and Au, a feature that is in particular visible for Au

in the BN-hollow site. The electron densities for the energy range from -4 to 0 eV [Fig. 5(b)] are very different. There is a large density around Au (evident also from the partial DOS in Fig. 4), and between Au and B there is always a strong bonding interaction, while between N and Au we observe a clear minimum in the charge density, indicating predominantly antibonding character. This is in line with the fact that the favorable adsorption site of a Au atom is on top of B. The charge densities for states above the Fermi level are shown in Fig. 5(c) and indicate an antibonding character for all Au-(B, N) interactions.

The Au-BN interaction is not only of covalent character, but there is also a significant charge transfer. There is no unique way to assign charges to the different atoms in a compound, but here we use an integration over the atomic basins as defined by Bader³⁴ (a surface around a nucleus, where the flux $\nabla\rho\cdot\vec{n} = 0$ is zero). However, in this method, already the superposition of neutral densities can give a significant charge transfer and thus we take the difference between the self-consistent density and the density obtained from a simple superposition of neutral atomic densities. In that way, we can remove the part stemming from overlapping densities and obtain a more realistic estimate for the real charge transfer. For instance, in bulk $h\text{-BN}$, the superposition of neutral atomic charge densities leads to Bader charges of $\pm 1.50e^-$, while the self-consistent charges are $\pm 2.20e^-$ and thus the charge redistribution due to chemical bonding is with $0.70e^-$ significantly smaller than the bare Bader charges. If a gold atom adsorbs on bulk $h\text{-BN}$, there is a small charge transfer of about $0.1e^-$ and the Au atom gets slightly negatively charged. The charge transfer is largest for Au on top of N and a bit smaller for other sites. A similar small charge transfer toward Au was also found for the Au/graphene system.³³ On the other hand, when Au adsorbs on the $h\text{-BN}/\text{Rh}(111)$ nanomesh, there is a significantly larger charge transfer (about $-0.7e^-$ for Au on B top, but only about $-0.5e^-$ for the other Au positions). The charge is coming predominantly from the N and B atoms nearest to the Au atom.

The model calculations presented above clearly indicate that the most favorable Au adsorption site is on top of the B atom when BN is in the bonding (fcc,top) position above Rh. This would predict that Au adsorption in the nanomesh pores is most favorable, and we have verified this conclusion by a few calculations using the full 13×12 $h\text{-BN}/\text{Rh}(111)$ nanomesh unit cell. In these cases, Au was placed at the optimal B_{top} site in the center of the nanomesh pore [corresponding to the B-top/ $BN(\text{fcc,top})/\text{Rh}(111)$ configuration of the 4×4 model supercell]. The calculation has been performed using the WC exchange-correlation functional and the optimization was carried out until the changes in the positions between two geometric iteration steps was below 0.01 \AA . The calculated binding energy is around 2.4 eV, which is a bit larger than from the (4×4 supercell) model calculations (1.98 eV). The vertical displacement of the B and N atoms due to the presence of the Au is close to $+0.5$ and -0.05 \AA , respectively, while the distance between the Au atom and the nearest B and N is 2.16 and 2.96 \AA , respectively. The geometric changes induced by Au in the $h\text{-BN}$ nanomesh are very close to the results calculated with the smaller 4×4 supercell (Table II). Actually, the geometric differences due to the use of the WC or

LDA functional for the 4×4 Rh(111) $_{h\text{-BN}}$ unit cell are already bigger than between the 13×12 $h\text{-BN/Rh(111)}$ nanomesh unit cell and the much smaller 4×4 $h\text{-BN/Rh(111)}$ $_{h\text{-BN}}$ unit cell when using the identical functional, which justifies its usage for the screening of possible interaction sites.

Widmer *et al.*²⁴ have reported that the preferred adsorption site of Xe atoms is at the rim of the pores due to the strong electric field present there. It should be noted that the adsorption mechanism of Xe and Au on the nanomesh is very different as the adsorption of Xe is driven solely by van der Waals interactions. In order to verify that for Au some strong covalent interactions dominate, and since it is not possible to describe the rim of the pores by some small model systems, we have also calculated the adsorption of the Au atom on the rim of the full 13×12 $h\text{-BN/Rh(111)}$ nanomesh. The resulting adsorption energy of 2.00 eV (WC-GGA) is smaller than the one calculated in the center of pore (2.40 eV at the B_{top} site) and indicates that Au atoms should be trapped in the pores and the adsorption mechanism of Au is different from that of Xe.

V. CONCLUSION

We have shown above that the Au atom binds to the $h\text{-BN/Rh(111)}$ nanomesh. This interaction is indeed much stronger than to the bulk $h\text{-BN}$. Moreover, the adsorption seems to be selective with respect to the regions of the nanomesh structure. Clearly, the nanomesh pore regions seems to be the preferred site for the adsorption in this case. More specifically, the Au atom binds strongest to the B atom, when $h\text{-BN}$ is close to the (fcc,top) configuration on Rh(111) and bonding should be so strong that the atoms are fairly immobilized at not too high temperatures. The binding mechanism involves hybridization of the $Au-d_{z^2}$ with $B-p_z$ orbitals and an additional charge transfer toward Au. For the less stable N-top and hollow adsorption sites, the $Au-d_{xz},d_{yz}$ orbitals participate also in the bond formation.

ACKNOWLEDGMENTS

The authors acknowledge support by the Austrian Science Foundation (Project No. I 319-N20) and discussions with H. Over.

-
- ¹M. Paffett, R. Simonson, P. Papin, and R. Paine, *Surf. Sci.* **232**, 286 (1990).
- ²A. Nagashima, N. Tejima, Y. Gamou, T. Kawai, and C. Oshima, *Phys. Rev. B* **51**, 4606 (1995).
- ³A. Nagashima, N. Tejima, Y. Gamou, T. Kawai, and C. Oshima, *Phys. Rev. Lett.* **75**, 3918 (1995).
- ⁴E. Rokuta, Y. Hasegawa, K. Suzuki, Y. Gamou, C. Oshima, and A. Nagashima, *Phys. Rev. Lett.* **79**, 4609 (1997).
- ⁵C. Oshima and A. Nagishima, *J. Phys.: Condens. Matter* **9**, 1 (1997).
- ⁶G. B. Grad, P. Blaha, K. Schwarz, W. Auwärter, and T. Greber, *Phys. Rev. B* **68**, 085404 (2003).
- ⁷M. N. Huda and L. Kleinman, *Phys. Rev. B* **74**, 075418 (2006).
- ⁸A. B. Preobrajenski, A. S. Vinogradov, and N. Mårtensson, *Phys. Rev. B* **70**, 165404 (2004).
- ⁹A. B. Preobrajenski, A. S. Vinogradov, and N. Mårtensson, *Surf. Sci.* **582**, 21 (2005).
- ¹⁰M. Corso, W. Auwärter, M. Muntwiler, A. Tamai, T. Greber, and J. Osterwalder, *Science* **303**, 217 (2004).
- ¹¹S. Berner *et al.*, *Angew. Chem., Int. Ed. Engl.* **46**, 5115 (2007).
- ¹²H. Dil, J. Lobo-Checa, R. Laskowski, P. Blaha, S. Berner, J. Osterwalder, and T. Greber, *Science* **319**, 1824 (2008).
- ¹³R. Laskowski, P. Blaha, T. Gallauner, and K. Schwarz, *Phys. Rev. Lett.* **98**, 106802 (2007).
- ¹⁴R. Laskowski and P. Blaha, *J. Phys.: Condens. Matter* **20**, 064207 (2008).
- ¹⁵R. Laskowski, P. Blaha, and K. Schwarz, *Phys. Rev. B* **78**, 045409 (2008).
- ¹⁶A. Goriachko, Y. He, M. Knapp, and H. Over, *Langmuir* **23**, 2928 (2007).
- ¹⁷M. Morscher, M. Corso, T. Greber, and J. Osterwalder, *Surf. Sci.* **600**, 3280 (2006).
- ¹⁸M. Corso, T. Greber, and J. Osterwalder, *Surf. Sci.* **577**, L78 (2005).
- ¹⁹A. T. N'Diaye, S. Bleikamp, P. J. Feibelman, and T. Michely, *Phys. Rev. Lett.* **97**, 215501 (2006).
- ²⁰S. Marchini, S. Günther, and J. Wintterlin, *Phys. Rev. B* **76**, 075429 (2007).
- ²¹A. B. Preobrajenski, M. L. Ng, A. S. Vinogradov, and N. Mårtensson, *Phys. Rev. B* **78**, 073401 (2008).
- ²²T. Brugger, S. Günther, B. Wang, H. Dil, M.-L. Bocquet, J. Osterwalder, J. Wintterlin, and T. Greber, *Phys. Rev. B* **79**, 045407 (2009).
- ²³A. Geim and K. Novoselov, *Nat. Mater.* **6**, 183 (2007).
- ²⁴R. Widmer, D. Passerone, T. Mattle, H. Sachdev, and O. Gröning, *Nanoscale* **2**, 502 (2010).
- ²⁵A. Goriachko, Y. He, and H. Over, *J. Phys. Chem. C* **112**, 8147 (2008).
- ²⁶I. Brihuega, C. Michaelis, J. Zhang, S. Bose, V. Sessi, J. Honolka, M. Schneider, A. Enders, and K. Kern, *Surf. Sci.* **602**, L95 (2008).
- ²⁷G. K. H. Madsen, P. Blaha, K. Schwarz, E. Sjöstedt, and L. Nordström, *Phys. Rev. B* **64**, 195134 (2001).
- ²⁸P. Blaha, K. Schwarz, G. K. H. Madsen, D. Kvasnicka, and J. Luitz, *WIEN2K: An Augmented Plane Wave and Local Orbitals Program for Calculating Crystal Properties*, ISBN 3-9501031-1-2 (Vienna University of Technology, Austria, 2001).
- ²⁹Z. Wu and R. E. Cohen, *Phys. Rev. B* **73**, 235116 (2006).
- ³⁰F. Tran, R. Laskowski, P. Blaha, and K. Schwarz, *Phys. Rev. B* **75**, 115131 (2007).
- ³¹P. Haas, F. Tran, and P. Blaha, *Phys. Rev. B* **79**, 085104 (2009).
- ³²R. Laskowski and P. Blaha, *Phys. Rev. B* **81**, 075418 (2010).
- ³³M. Amft, B. Sanyal, O. Eriksson, and N. Skorodumova, *J. Phys.: Condens. Matter* **23**, 205301 (2011).
- ³⁴R. Bader, *Atoms in Molecules: A Quantum Theory* (Oxford University Press, Oxford, UK, 1990).